Structural properties and quasiparticle band structure of zirconia

Balázs Králik, Eric K. Chang, and Steven G. Louie
Department of Physics, University of California at Berkeley, Berkeley, California 94720
and Materials Science Division, Ernest Orlando Lawrence Berkeley National Laboratory, Berkeley, California 94720
(Received 27 October 1997)

We report *ab initio* calculations of the structural and quasiparticle properties of ZrO_2, otherwise known as zirconia. The plane-wave pseudopotential method is used to compute the structural properties of the cubic, tetragonal, and monoclinic phases of zirconia. Oxygen vacancies in the cubic phase are also studied using a supercell approach. The structural parameters, including all internal degrees of freedom of all phases, are relaxed. Excellent agreement is achieved with experiment and with other *ab initio* calculations available. We compute the quasiparticle band gaps within Hedin's *GW* approximation using the method of Hybertsen and Louie, and confirm that the quasiparticle approach can be successfully applied to transition-metal oxides if the core-valence overlap is small. We predict the fundamental gap of pure cubic, tetragonal, and monoclinic zirconia to be 5.55 eV, 6.40 eV, and 5.42 eV, respectively. Within the *GW* approximation, the oxygen vacancy state in the cubic phase is found to be nondegenerate, fully occupied, and well separated from the valence and conduction bands, positioned 2.1 eV below the conduction band edge. [S0163-1829(98)00112-X]

I. INTRODUCTION

Zirconia is a technologically very important material[1,2] which can be used in practical applications not only as a structural ceramic but also, for example, as an important component in catalytic converters, in oxygen sensors, and in chemically passivating surfaces. The latter applications require a thorough understanding of the electronic properties of this material.

The electronic and structural properties of zirconia have been studied before in detail within the *ab initio* density-functional-theory–local-density approximation (DFT-LDA)[3] and *ab initio* Hartree-Fock[4] methods. However, these methods are known not to be predictive for excited state properties such as the band gap. Clearly, for an understanding of the chemical and electronic properties of zirconia, a predictive calculation of its excited state properties is necessary.

The *GW* approximation for the electron self-energy, first described systematically by Hedin[5] and first developed as a practical computational approach for real materials by Hybertsen and Louie,[6,7] is the state-of-the-art method for predictive calculations of the band gap and of other excited-state properties. It has yielded excellent results for semiconductors and insulators.[8] However, until recently the method has remained to be proven valid for *d*-electron systems, such as ZrO_2. Motivated by the recent success of Rohlfing, Kruger, and Pollmann for CdS,[9] we applied the *GW* method for calculations of the quasiparticle band structure of ZrO_2. Our results, as we will show below, are in good agreement with the available experimental data.[3]

The paper is organized as follows. First, we study the structural properties of the phases of ZrO_2 within the pseudopotential DFT-LDA formalism. The success of this method in predicting structural properties of ZrO_2 is in itself important, because the plane wave pseudopotential method is simple and very efficient in exploring structural transitions. Second, having verified the applicability of the pseudopotential plane wave method to the ground state of ZrO_2, we then use the calculated pseudo wave functions to compute the quasiparticle band structure of cubic zirconia with the *GW* approximation. Our work is of particular theoretical importance because it constitutes one of the first *GW* calculations for systems in which *d*-electrons play an important role, and it sheds light on the applicability of the *GW* approximation to such systems. Successful first-principles quasiparticle calculations on transition-metal compounds have been performed only recently.[9–12] Finally, we study the electronic structure of an oxygen vacancy in cubic zirconia. Oxygen vacancies are believed to be instrumental in the structural stabilization of zirconia. They also make zirconia useful as an oxygen ion conductor.

II. CALCULATION OF STRUCTURAL PROPERTIES

Structural properties of ZrO_2 are determined using density-functional theory within the local-density approximation (LDA).[13,14] We expand the valence pseudo wave functions in a plane wave basis set up to a cutoff of 100 Ry to obtain fully converged results. This corresponds to approximately 16 000 plane waves for the monoclinic phase, which has the largest unit cell. Brillouin zone summations are carried out using a Monkhorst-Pack grid with ten, six, and two *k* points in the irreducible zone for the cubic, tetragonal and monoclinic phases, respectively. The plane-wave cutoff and *k*-point sampling are sufficient for full convergence in the Hellman-Feynman forces and stress. Atomic coordinates and lattice parameters were varied until the forces and stress vanished. The structural minimization is carried out using a quasi-Newton method.[15] A fully converged, self-consistent relaxation of all the 13 structural parameters of the monoclinic phase can be performed in less than 10 h on 32 processors of a Cray T3E.

Throughout this study we made use of the pseudopotential approximation. The oxygen pseudopotentials are generated using the Troullier-Martins scheme[16] whereas the zirconium is treated using Hamann-Schluter-Chiang potentials.[17] For

TABLE I. Structural properties of hcp metallic Zr. Figures in parentheses give the percent error as compared to experiment. We present pseudopotential LDA calculations with Ceperley-Alder exchange-correlation [PP(CA)] (present work) and all-electron linearized augmented plane-wave LDA with Hedin-Lundquist exchange-correlation [LAPW(HL)] (from Ref. 33). Volumes per formula unit and lattice parameters are in atomic units. Experimental data are from Refs. 34 and 35.

	PP(CA)	LAPW(HL)	Expt.
Volume	147.89(−5.7%)	147.84(−5.9%)	157.05
c/a	1.629(+2.3%)	1.627(+2.1%)	1.593
a	5.940(−2.7%)	5.943(−2.6%)	6.104
c	9.679(−0.5%)	9.668(−0.6%)	9.723

oxygen we make the usual choice of including the six electrons in the $N=2$ shell as valence electrons. For zirconium, all electrons in the $N=4$ shell plus the $5s$ subshell in the atomic configuration ($4s^2 4p^6 4d^2 5s^2 = 12$ electrons) are included among the valence bands. We have tried to reduce the number of valence electrons by only treating the $5s$ and $4d$ as valence electrons, but this leads to unsatisfactory equilibrium lattice parameters for cubic ZrO_2.

For structural calculations, we further convert the semilocal pseudopotentials described above to the fully nonlocal form of Kleinman and Bylander.[18] The Kleinman-Bylander (KB) form of the pseudopotentials is separable and hence allows considerable savings in computational effort. We take the d and p channels as the local potentials for zirconium and oxygen, respectively. With these choices, the pseudopotentials are transferable including the low-lying conduction bands (see Table I). For band structure and GW calculations, we do not use the KB procedure because of the possibility of encountering *ghost states*.[19]

The inclusion of $4s$ and $4p$ electrons in the valence shell of Zr is important for reasons other than their effect on the structural properties. Even though the $4d$, $4s$, and $4p$ atomic energy levels are tens of eVs apart from each other, the corresponding atomic wave functions strongly overlap (see Fig. 1). As shown by Rohlfing, Kruger, and Pollmann,[9] in a case such as this, one does not obtain accurate quasiparticle energies unless all of the strongly spatially overlapping orbitals are treated on an equal footing.

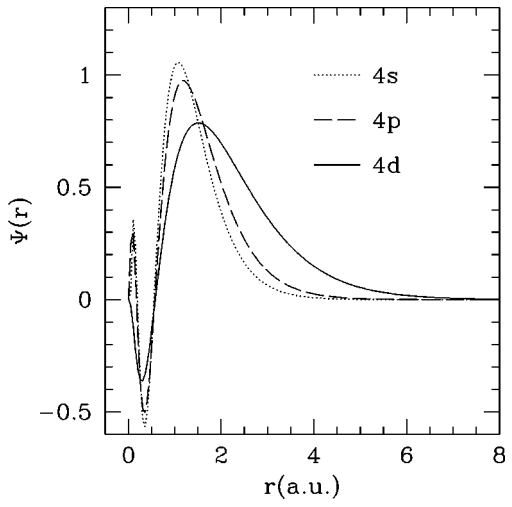

FIG. 1. Atomic wave functions of the 4 shell of the Zr atom.

III. CALCULATION OF QUASIPARTICLE ENERGIES

In this section, we summarize the basic ideas of the GW approximation for quasiparticle properties. The GW approximation was first proposed by Hedin.[5] In practice, we follow the scheme for semiconductors, due to Hybertsen and Louie.[6,7] The method is based on an approximate solution to the quasiparticle equation[20]

$$(T+V_{\text{ext}}+V_h)\Psi_{n\mathbf{k}}(\mathbf{r})+\int d^3\mathbf{r}'\Sigma(\mathbf{r},\mathbf{r}';E_{n\mathbf{k}})\Psi_{n\mathbf{k}}(\mathbf{r}') = E_{n\mathbf{k}}\Psi_{n\mathbf{k}}(\mathbf{r}), \tag{1}$$

where T is the kinetic energy operator ($-\frac{1}{2}\nabla_{\mathbf{r}}^2$ in atomic units), V_{ext} is the external (ionic) potential, V_h is the Hartree potential due to the average Coulomb repulsion of the electrons, and Σ is the self-energy operator. Σ is in general a nonlocal, energy-dependent, non-Hermitian operator that describes exchange and correlation (dressing) effects on the quasiparticle states. In addition, the non-Hermitian part of Σ gives rise to a finite lifetime for the quasiparticles. Near the Fermi level, however, lifetime effects can be, and, as usual, are neglected in the interpretation of peak positions in experimental excitation spectra.

The quasiparticle equation is similar to the familiar self-consistent field equation in the Kohn-Sham formulation of density-functional theory (DFT) (Refs. 13,14),

$$(T+V_{\text{ext}}+V_h+V_{xc})\psi_{n\mathbf{k}}(\mathbf{r})=\epsilon_{n\mathbf{k}}\psi_{n\mathbf{k}}(\mathbf{r}) \tag{2}$$

if we set $\Sigma^{\text{LDA}}=\delta(\mathbf{r},\mathbf{r}')V_{xc}(\mathbf{r}')$. While the Kohn-Sham eigenvalues $\epsilon_{n\mathbf{k}}$ only have meaning as Lagrangian multipliers, and in particular cannot be interpreted exactly as excitation energies, the above analogy suggests that $\epsilon_{n\mathbf{k}}$ can in fact be considered as a first approximation to quasiparticle energies. (Similarly, one can consider the eigenvalues of the Hartree-Fock equation as approximate quasiparticle energies.)

It is natural then to try to obtain the true quasiparticle levels and wave functions perturbatively from the Kohn-Sham (or Hartree-Fock) eigenvalues and eigenfunctions. Within this approach, the perturbation operator is $H_1=\Sigma(E)-V_{xc}$. Assuming for the moment that we know Σ, we can immediately write down the first-order result

$$E_{n\mathbf{k}}=\epsilon_{n\mathbf{k}}+\frac{\langle\psi_{n\mathbf{k}}|\Sigma(E_{n\mathbf{k}})-V_{xc}|\Psi_{n\mathbf{k}}\rangle}{\langle\psi_{n\mathbf{k}}|\Psi_{n\mathbf{k}}\rangle}. \tag{3}$$

In practice H_1 is found to be virtually diagonal in the $\{\psi_{n\mathbf{k}}\}$ basis for semiconductors[6] such as Si, Ge, CdS,[9] and ZrO_2, so we in fact take

$$\Psi_{n\mathbf{k}}=\psi_{n\mathbf{k}} \tag{4}$$

and

$$E_{n\mathbf{k}}=\epsilon_{n\mathbf{k}}+\langle\psi_{n\mathbf{k}}|\Sigma(E_{n\mathbf{k}})-V_{xc}|\psi_{n\mathbf{k}}\rangle. \tag{5}$$

We next consider evaluating the operator Σ. Following Hybertsen and Louie,[6] the operator $\Sigma(E)$ can be approximated in the GW approximation[5] as

$$\Sigma(\mathbf{r},\mathbf{r}';E)=i\int\frac{d\omega'}{2\pi}e^{-i\delta\omega}G(\mathbf{r},\mathbf{r}';E-\omega')W(\mathbf{r},\mathbf{r}';\omega'), \tag{6}$$

where δ is a positive infinitesimal, G is our best available Green's function, and W is the best available screened Coulomb interaction. Both G and W are evaluated with the LDA wave functions. Accordingly, G is taken to the Green's function formed from the LDA orbitals:

$$G(\mathbf{r},\mathbf{r}',\omega)=\sum_{n\mathbf{k}}\frac{\psi_{n\mathbf{k}}(\mathbf{r})\psi^*_{n\mathbf{k}}(\mathbf{r}')}{\omega-E_{n\mathbf{k}}-i\delta_{n\mathbf{k}}}, \tag{7}$$

where $\delta_{n\mathbf{k}}=0^+$ for $E_{n\mathbf{k}}<\mu$ and $\delta_{n\mathbf{k}}=0^-$ for $E_{n\mathbf{k}}>\mu$. The $\epsilon_{n\mathbf{k}}$ are initially taken to be the LDA eigenvalues and are subsequently updated upon repeated iterations of the self-consistent equation Eq. (5).

$W(\mathbf{r},\mathbf{r}';\omega)$ is computed using RPA dielectric screening at $\omega=0$, and then extended to finite frequencies using a generalized plasmon-pole model, as described by Hybertsen and Louie.[6] Before we proceed, let us fix the Fourier transform convention for the spatial coordinates in a crystal to mean

$$f(\mathbf{r},\mathbf{r}';\omega)=\sum_{\mathbf{q},\mathbf{G},\mathbf{G}'}e^{i(\mathbf{q}+\mathbf{G})\cdot\mathbf{r}}f_{\mathbf{G}\mathbf{G}'}(\mathbf{q},\omega)e^{-i(\mathbf{q}+\mathbf{G}')\cdot\mathbf{r}'}, \tag{8}$$

where $\mathbf{q}$ is a wave vector in the first Brillouin zone and $\mathbf{G}$ is a reciprocal lattice vector. In terms of the LDA wave functions, the RPA irreducible polarizability is given (in $\mathbf{r},t$ space) by

$$P^0(\mathbf{r},t;\mathbf{r}',t')=-iG(\mathbf{r},t;\mathbf{r}',t'+\delta)G(\mathbf{r}',t';\mathbf{r},t). \tag{9}$$

From this expression, the dielectric function (in $\mathbf{q},\omega$ space)

$$\epsilon_{\mathbf{G}\mathbf{G}'}(\mathbf{q},\omega)=\delta_{\mathbf{G}\mathbf{G}'}-v^{\mathrm{Coul}}(\mathbf{q}+\mathbf{G})P^0_{\mathbf{G}\mathbf{G}'}(\mathbf{q},\omega) \tag{10}$$

can be obtained. The screened interaction is given by

$$W_{\mathbf{G}\mathbf{G}'}(\mathbf{q},\omega)=\epsilon^{-1}_{\mathbf{G}\mathbf{G}'}(\mathbf{q},\omega)v^{\mathrm{Coul}}(\mathbf{q}+\mathbf{G}'). \tag{11}$$

The preceding discussion is general. In our implementation, we make a further approximation and evaluate $\epsilon_{n\mathbf{k}}$ and $\psi_{n\mathbf{k}}$ within a pseudopotential DFT-LDA scheme. The pseudopotential approximation requires us to fix some of the contributions to the self-energy operator.

In order to understand the approximations resulting from the use of pseudopotentials, let us decompose G into two terms, $G=G_c+G_v$, where G_c only involves the core orbitals and G_v involves the rest of the valence orbitals and the conduction states. Similarly, the polarizability P can be decomposed into parts involving virtual transitions from core bands to conduction bands (P_c) and parts involving transitions from valence to conduction bands (P_v). Assuming $P_c \ll P_v$ we get

$$\Sigma=iG_cW+iG_vW_vP_cW_v+iG_vW_v. \tag{12}$$

The first term corresponds essentially to the core-valence exchange energy, as noted by Phillips,[21] and the second term is a screened polarization potential due to the core. These two terms together correspond to a core-valence exchange-correlation energy. The third term is the self-energy of the valence electrons.

The first two terms of this equation are usually omitted from the calculations, because Hybertsen and Louie[6] have found that their contributions to excitation energies differ very little from the corresponding LDA values for bulk silicon and germanium. For these cases, the pseudopotential was chosen in such a way that the core and valence electrons resided on different shells, thereby ensuring a relatively small overlap between core and valence electrons. However, for the opposite case, i.e., when there is significant core-valence spatial overlap, the core-valence exchange-correlation contributions can be important, as Louie, Froyen, and Cohen[22] have pointed out in their work on the nonlinear core correction for *ab initio* pseudopotentials. Shirley, Zhu, and Louie[23] have shown that in certain shallow core semiconductors, core-valence exchange-correlation effects can change the gap by as much as 0.4 eV. In their work on CdS, Rohlfing, Kruger and Pollmann[9] have also shown that when core and valence orbitals overlap, the contributions from the core-valence exchange-correlation are different in LDA and in GW, respectively. Motivated by these observations, we have treated the $4s$, $4p$, $4d$, and $5s$ electrons as valence electrons for zirconium, and neglected the remaining core-valence exchange-correlation terms in the evaluation of quasiparticle energy differences.

IV. RESULTS AND DISCUSSION

A. Structural properties

Zirconia (ZrO_2) in its pure form and at zero pressure is monoclinic (m) up to 1170 °C, tetragonal (t) between 1170 and 2370 °C, cubic (c) between 2370 and 2706 °C, and molten above.[24] Dopants such as Y_2O_3, CaO, and MgO are known to stabilize the cubic and tetragonal phases at room temperature. The dopants introduce substitutional impurities at the zirconium sites and oxygen vacancies. At high temperatures and high concentrations, the vacancies are mobile.[25]

The high temperature c phase (space group $Fm3m$) is an fcc lattice of zirconium atoms with oxygen atoms at the tetrahedral sites. Consequently, the oxygen atoms and the zirconium atoms are tetrahedrally coordinated and octahedrally coordinated, respectively, and the unit cell contains one zirconium and two oxygen atoms. The cubic structure is fully determined by the single lattice constant.

The intermediate temperature t phase (space group $P4_2/nmc$) can be derived from the cubic phase by displacing the oxygen atoms along the c axis of the tetragonal unit cell. This displacement is accompanied by a readjustment of the lattice parameters. The lattice vectors meet at right angles, with two of them equal in length. The t phase is therefore characterized by two lattice constants and the displacement d_z of the oxygen atoms in the unit cell with respect to their cubic positions. The unit cell contains two formula units of ZrO_2. The mechanism of the cubic to tetragonal phase transition is described in detail in Refs. 26 and 27.

The low temperature monoclinic phase of ZrO_2 (space group $P2_1/c$) is formed by further distorting the tetragonal structure. With the lattice vectors no longer at right angles, the zirconium atoms are only sevenfold coordinated in this phase. There are two symmetry-inequivalent types of oxygen

TABLE II. Structural parameters of the phases ZrO_2. The full-potential linearized augmented plane-wave all-electron DFT-LDA (FLAPW) results are from Ref. 28 and the plane-wave pseudopotential DFT-LDA (PP) results are from the present work. The experimental results are taken from Ref. 25. The deviation from the experimental result, expressed as a percentage, is given in parentheses. Volumes per formula unit and lattice parameters are in atomic units. Internal coordinates are given in terms of the lattice vectors. In the tetragonal phase, d_z is the displacement of the oxygen along the z axis in units of c with respect to the ideal cubic position.

	PP(this work)	FLAPW	Expt.
	Cubic ZrO_2		
Volume	215.31(−3.2%)	217.79(−2.1%)	222.48
a	9.514(−1.1%)	9.551(−0.7%)	9.619
	Tetragonal ZrO_2		
Volume	218.69(−1.9%)	218.77(−1.9%)	222.96
a	9.523(−0.2%)	9.541(+0.0%)	9.543
c	9.646(−1.5%)	9.613(−1.8%)	9.793
d_z	0.0423(−26.3%)	0.029(−49.5%)	0.0574
	Monoclinic ZrO_2		
Volume	230.51(−3.0%)		237.71
a	9.611(−1.3%)		9.734
b	9.841(−0.0%)		9.849
c	9.876(−1.7%)		10.048
γ	99.21(−0.0%)		99.23
x_{Zr}	0.2779(+0.9%)		0.2754
y_{Zr}	0.0418(+5.8%)		0.0395
z_{Zr}	0.2099(+0.7%)		0.2083
$x_{O(1)}$	0.0766(+9.4%)		0.0700
$y_{O(1)}$	0.3488(+5.1%)		0.3317
$z_{O(1)}$	0.3311(−3.9%)		0.3447
$x_{O(2)}$	0.4471(−0.5%)		0.4496
$y_{O(2)}$	0.7588(−0.3%)		0.7569
$z_{O(2)}$	0.4830(−0.8%)		0.4792

atoms, one threefold, the other fourfold coordinated. We need 13 independent parameters to describe this structure. The data presented in Table II for the monoclinic phase correspond to the second setting convention for monoclinic crystals. The unit cell contains four formula units of ZrO_2.

Table II summarizes the results of our structural studies on the three phases of ZrO_2. There is excellent agreement between the results of our pseudopotential plane wave method and those of the all-electron FLAPW method.[28] The theoretical lattice parameters are also in excellent agreement with experiment. The success of the pseudopotential treatment is in fact not surprising given the similar success of the *ab initio* Hartree-Fock treatment of zirconia within the effective core potential (ECP) approximation.[25,4]

Table III shows the total energies of the pure phases. The energies quoted are cohesive energies, i.e., differences of total energies per molecular unit and the energies of the constituent pseudoatoms. We find that the ordering of the cohesive energies follows the one suggested by their temperature ordering:

$$E_m < E_t < E_c . \tag{13}$$

TABLE III. Cohesive energies(E_{coh}) of the pure phases of ZrO_2 given in Rydbergs/ZrO_2. The third column shows the total energy difference between the phases and the cubic phase. The fourth column contains the corresponding experimental values from Ref. 29.

Phase	E_{coh}	$E_c - E_{t,m}$	Expt.
cubic	1.5331		
tetragonal	1.5364	0.0033	0.0042
monoclinic	1.5406	0.0075	0.0088

Our calculated values are in fact in excellent quantitative agreement with experiment. The experimental values for the energy differences were derived from measured enthalpy differences at the phase transition temperature.[29]

B. Electronic properties

1. Cubic phase

We first examine the electronic structure of the cubic phase within our pseudopotential LDA method. We perform the electronic structure calculations at the experimental lattice parameters. Figure 2 shows the total and partial density of states for this phase. The partial density of states (DOS) at energy E at atom X with angular momentum l,m is obtained by examining the wave functions with energy eigenvalue E. The partial density of states $D_{Xl}(E)$ at atom X and angular momentum l is given by

$$D_{Xl}(E) = \sum_m \sum_{n\mathbf{k}}^{\text{occ}} |\langle \theta(|\mathbf{r}-\mathbf{r}_X| < r_c) Y_{lm}(\vartheta,\psi) | \psi_{n\mathbf{k}} \rangle|^2 \times \delta(\epsilon_{n\mathbf{k}} - E), \tag{14}$$

where $\mathbf{r}_X$ denotes the position of the atom at which the partial density of states is computed, and $\theta(|\mathbf{r}-\mathbf{r}_X| < r_c)$ is a step function equal to unity for values of $|\mathbf{r}-\mathbf{r}_X|$ less than the radius cutoff r_c and zero otherwise. The angular decomposition shows that the top of the valence band is formed from O $2p$ orbitals and the semicore bands, in order of decreasing energy, are O $2s$ and Zr $4p$ bands. It is interesting to note

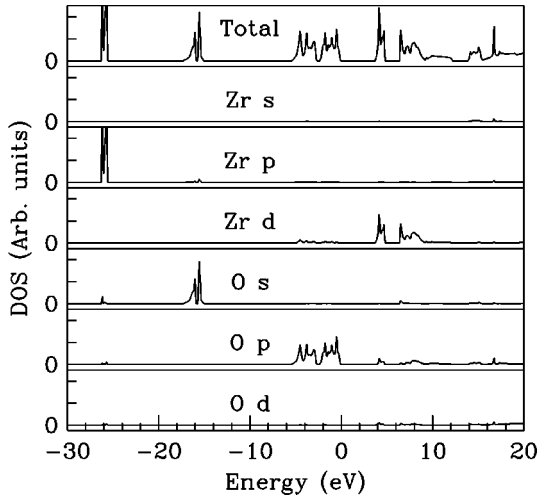

FIG. 2. Angular resolved local density of states of cubic zirconia. The zero of the x axis is the Fermi level.

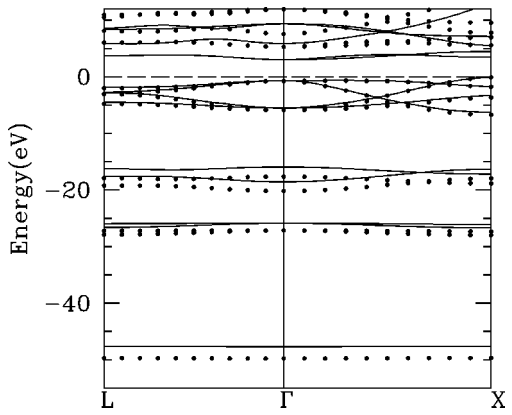

FIG. 3. Band structure of cubic zirconia. Continuous lines represent the LDA band structure, while dots show the *GW* quasiparticle bands. The two sets of bands are aligned at the top of the valence band, which was set to 0.

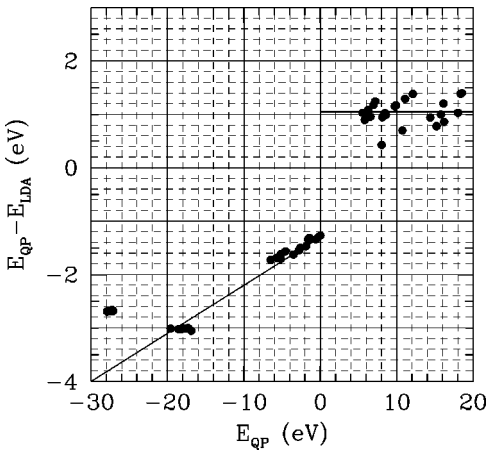

FIG. 4. Quasiparticle correction versus LDA band energy for cubic zirconia. The zero of the energy is set at the top of the valence band.

that there are no Zr *s*- and *d*-character states in the valence bands (except for the deep semicore Zr 4*s* states, which are not shown). This suggests a nearly complete transfer of the Zr 5*s* and 4*d* electrons to the oxygen atoms in the crystal.

For the *GW* calculation, the LDA wave functions $\psi_{n\mathbf{k}}$, and energies $\epsilon_{n\mathbf{k}}$ are obtained using semilocal pseudopotentials, i.e., not the fully separable Kleinman-Bylander pseudopotentials. This comes at a performance cost, but gives us the advantage of avoiding the issue of ghost states in the conduction band. Bands up to energies 250 eV above the fundamental gap are included in the summation over conduction bands. The wave functions are expanded up to a plane-wave cutoff of 60 Ry. The quasiparticle energies and the gaps were fully converged at this cutoff. (We find that at 40 Ry the quasiparticle energies are converged to 0.2 eV, and the gaps are systematically underestimated by 0.15 eV.) The dielectric constant is computed to a reciprocal space cutoff of 4 a.u.

Figure 3 shows the quasiparticle band structure of cubic zirconia. The self-energies of states at generic *k* points are obtained by linear interpolation of the calculated values at nearby high-symmetry points of the Brillouin zone. See Ref. 3 for the notation for all of the high-symmetry points in the Brillouin zones for the cubic, tetragonal, and monoclinic phases. We observe, due to the self-energy correction, a lowering and widening of the O 2*p* valence band and an approximate constant ''scissors'' shift upward of the conduction bands. The minimum gap is indirect from *X* to Γ in both the LDA and *GW* calculations.

Figure 4 shows the quasiparticle corrections to the LDA eigenvalues for the cubic phase. The corrections to the valence band follows very closely the trend seen in other semiconductors.[6] There is also a lowering of energy. However, this may be due to inconsistent comparison of Ceperly-Alder exchange correlation with *GW* exchange-correlation. The lowest conduction band is corrected uniformly over the Brillouin zone with a state dependence of about 0.1 eV. Higher conduction bands show nonuniform state-dependent corrections with up to about 1 eV variation over the Brillouin zone.

In Fig. 5, we compare our theoretical valence band density of states with the x-ray photoemission spectra (XPS) measured by French *et al.*[3] The experimental results shown are for a 9.5 mol % Y_2O_3-stabilized single crystal cubic ZrO_2 sample. While pure cubic zirconia has an experimental lattice constant (obtained from extrapolation from high-temperature values) of 9.619 a.u., the stabilized sample had $a=9.719$ a.u. Repeating the calculation at the larger lattice constant yields a gap that is 0.1 eV smaller and an O 2*p* valence band that is 0.3 eV narrower. The theoretical DOS curves shown in Fig. 5, calculated for a pure sample at $a=9.619$, are broadened by the experimental resolution of 0.7 eV.

In the energy range shown, the three main features in the theoretical curve are the O 2*p* valence and the O 2*s* and Zr 4*p* semicore bands. The *GW* correction proves to be very important in obtaining the correct peak positions for the semicore states. In particular, a shift of ~ 2 eV is observed for the O 2*s* peak. The valence bandwidth is slightly increased by the quasiparticle correction, and agrees well with the experiment. The experimental feature marked Y 4*p* has been identified as impurity related by examining spectra with different dopant concentrations. Based on our calculations, we are unable to identify features A and B with any structure in the electronic structure of pure cubic ZrO_2. Thus we propose that they are also defect related.

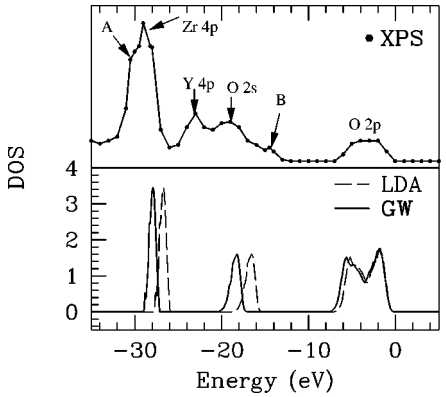

FIG. 5. Comparison of calculated and experimental valence density of states (DOS). The experimental values (in arbitrary units) are from the XPS measurements of Ref. 3. The calculated density of states are given in units of states/unit cell/spin/eV.

TABLE IV. Valence band maxima (VBM) and conduction band minima (CBM) of tetragonal ZrO_2 at selected high-symmetry points of the Brillouin zone. The calculations were carried out at 40 Ry plane wave cutoff. The *GW* estimate column shows the calculation of the tetragonal bandgap using the energy-dependent *GW* correction obtained from a 40 Ry calculation in the cubic phase. The LDA energy of the VBM at the *Z* point has been set to zero.

k point		LDA(40 Ry)	*GW*(40 Ry)	*GW* estimate
Γ	VBM	−0.03	−1.28	−1.23
	CBM	4.01	5.12	5.06
Z	VBM	0.00	−1.19	−1.20
	CBM	4.60	5.79	5.65
R	VBM	−0.82	−2.12	−2.09
	CBM	4.55	5.68	5.60
X	VBM	−0.03	−1.26	−1.23
	CBM	4.44	5.51	5.49
M	VBM	−0.56	−1.78	−1.81
	CBM	5.19	6.45	6.24

2. Tetragonal and monoclinic phases

Performing a fully converged *GW* calculation on the tetragonal and monoclinic phases of zirconia would be too expensive computationally. Instead, we only compute an LDA band structure for these phases (at the experimental structure) and use the *GW* self-energy corrections obtained in the cubic phase to correct the LDA eigenvalues. In this scheme, we assume that for all phases of ZrO_2 the quasiparticle correction of the energy of any state is given by the interpolation curves in Fig. 4. All states at the same energy are treated as having the same *GW* quasiparticle correction, which amounts to neglecting **k** dependence of $\Sigma - V_{xc}$. This approximation reproduces the quasiparticle correction to better than 0.05 eV accuracy near the gap (see Fig. 4) in the cubic phase. Test calculations in which we compare the interpolation formula with the exact *GW* results for the tetragonal phase at a lower, computationally feasible cutoff, confirm the applicability of this approximation (see Table IV).

Figures 6 and 7 show the *GW* quasiparticle band structures of the tetragonal and monoclinic phases, respectively.

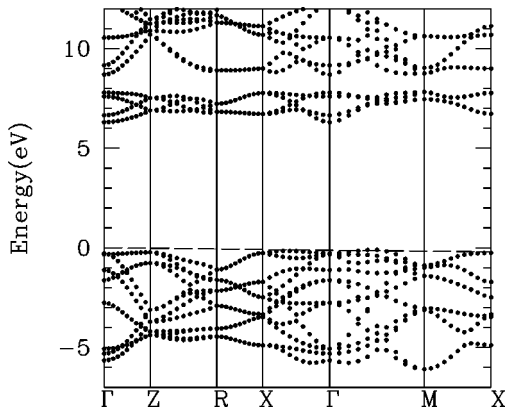

FIG. 6. *GW* quasiparticle band structure of tetragonal zirconia. (See text.)

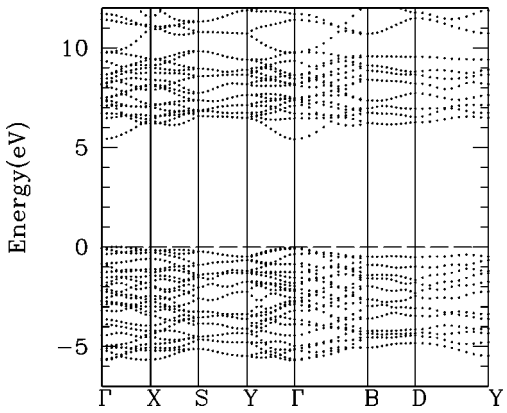

FIG. 7. *GW* quasiparticle band structure of monoclinic zirconia. (See text.)

Both phases are wide bandgap semiconductors, with an indirect fundamental gap. The minimum of the conduction band is at Γ for both phases, and the minimum optical (direct) gap is also located at the zone center. The valence band maxima fall on the Σ symmetry line (between Γ and *M*) for the tetragonal phase and between Γ and *X* for the monoclinic phase.

3. Band gaps and bandwidths

We present our calculated minimum bandgaps and valence bandwidths in Table V. Our LDA values are in reasonable overall agreement with the earlier results of Zandiehnadem, Murray, and Ching.[30] Since these 1988 results were computed non-self-consistently for the tetragonal and monoclinic phases, we do not expect them to agree closely with our self-consistent results.

Both the bandwidths and the bandgaps are systematically overestimated in the Hartree-Fock (HF) calculations of Orlando *et al.*[4] This is not surprising, as it is well known that HF calculations systematically overestimate and LDA calculations underestimate the fundamental gap of semiconductors. Indeed, our *GW* results, which agree well with experiment, are between the LDA and HF values for both the fundamental gap and the valence bandwidth.

Table VI shows the gaps as measured by vacuum ultraviolet (VUV) spectroscopy.[3] These gaps were derived from reflectance spectra through Kramers-Kronig[31] analysis. The

TABLE V. Minimum band gaps and valence bandwidths (in eV) of ZrO_2 compared to other *ab initio* calculations.

		This work			
	Phase	LDA	*GW*	HF[a]	LCAO[b]
Band gap	cubic	3.25	5.55	12.3	3.84
	tetragonal	4.10	6.40	13.3	4.11
	monoclinic	3.12	5.42		4.51
Valence bandwidth	cubic	6.1	6.5	7.97	5.90
	tetragonal	5.4	5.9	7.14	5.48
	monoclinic	5.2	5.7		4.97

[a] *Ab initio* Hartree-Fock calculation from Ref. 4.

[b] *Ab initio* orthogonalized LCAO DFT-LDA calculation from Ref. 30. Only the cubic phase was computed self-consistently.

TABLE VI. Minimum band gaps of ZrO_2 compared to experiments.

Phase		LDA	*GW*	Expt.
cubic	direct	3.65	5.81	6.1–7.08[a]
	indirect	3.25	5.55	
tetragonal	direct	4.26	6.57	5.78–6.62[b]
	indirect	4.10	6.40	
monoclinic	direct	3.16	5.46	5.83–7.09[c]
	indirect	3.12	5.42	

[a]Cubic ZrO_2:9.5 mol% Y_2O_3, from Ref. 3.
[b]Tetragonal ZrO_2:4.5 mol% Y_2O_3, from Ref. 3.
[c]Monoclinic ZrO_2, from Ref. 3.

gaps extracted are sensitive to the details of the fitting procedure used. The range of experimental values indicated in Table VI corresponds to two different fits of the reflectance spectra, hence we estimate the experimental uncertainty to be as much as 1 eV.

It has also been suggested in Ref. 3 that gaps derived from VUV reflectance spectroscopy are too high. This observation is confirmed by photocurrent generation spectroscopy.[32] The latter method gives a gap value of 4.8 eV for anodic thin films of ZrO_2 of undetermined structure. While surface and defect effects could be important in the interpretation of this latter measurement, the results of the photocurrent experiment suggest that the VUV data might be too high.

Table VI also shows LDA and *GW* values for the gaps. We find that the *GW* approximation improves agreement between theory and experiment considerably. While the *GW* gaps are within the experimental uncertainty of the measured values, differences in the gap value for the different phases are not resolved experimentally.

V. OXYGEN VACANCY

In practical applications, zirconia is typically doped in such a way as to introduce oxygen vacancies into the crystal structure. This is because not only are oxygen vacancies responsible for the oxygen-ion conducting properties of this material, dopants also endow zirconia with improved mechanical properties.[1,2]

To study the nature of oxygen vacancies in cubic zirconia, we perform calculations on a supercell of seven oxygen atoms and four zirconium atoms, obtained by removing an oxygen atom from the conventional cell of cubic zirconia, shown in Fig. 8. Such a supercell consists of four formula units of ZrO_2 with one less oxygen atom and is four times the volume of the primitive cell of pure, cubic zirconia. We allow the internal coordinates of this supercell to relax while keeping the cell volume fixed at the experimental pure bulk cubic volume. The initial configuration of the relaxation is obtained by taking the above supercell and distorting it asymmetrically. We find that the crystal relaxes to a symmetric structure, with the Zr atoms moving a distance of 0.015 Å directly away from the vacancy. The LDA relaxations were carried out with a plane wave cutoff of 100 Ry and a $2\times2\times2$ Monkhorst-Pack grid in the Brillouin zone.

Figure 9 shows the LDA band structure of the supercell.

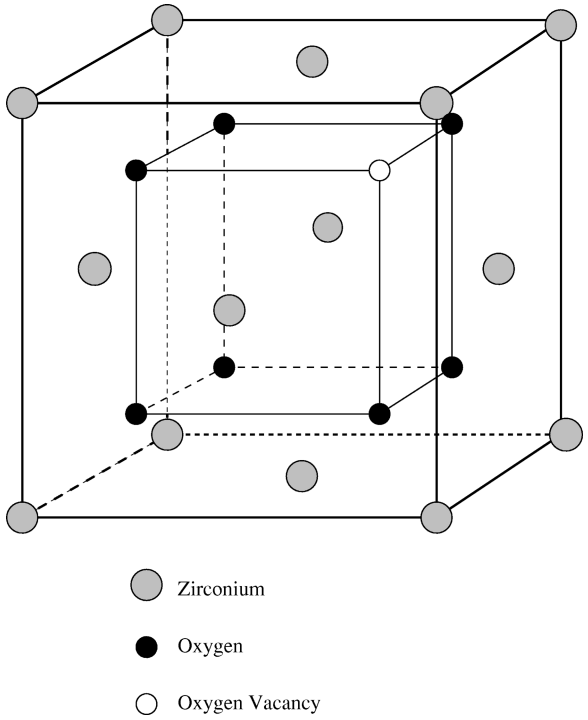

FIG. 8. Supercell used in the vacancy calculation.

The vacancy state, indicated by the dashed line, is singly degenerate, fully occupied, and well separated from both the valence bands and the conduction bands. Its dispersion throughout the Brillouin zone is approximately 1 eV, indicating an appreciable vacancy-vacancy interaction. We make the following observations to explain the above vacancy band structure in a tight-binding picture. First, by removing an oxygen atom, we remove the O 2*s*- and 2*p*-like orbitals previously present at the vacancy site. Therefore, if in the folded Brillouin zone scheme for the pure crystal, there are (8×3) O 2*p* and (8×1) O 2*s* filled bands, we expect there to be (7×3) O 2*p* and (7×1) O 1*s* filled bands in the crystal supercell with oxygen vacancy, which is precisely the result we obtain. Second, in the crystal, the O atoms borrow approximately two electrons from the surrounding four Zr atoms. Thus, by removing an oxygen atom, we remove six electrons, leaving two electrons behind which occupy the

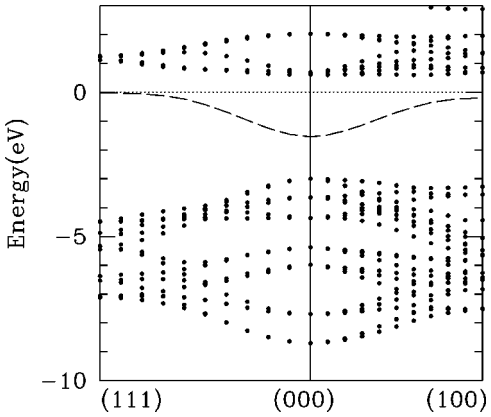

FIG. 9. LDA band structure of cubic zirconia with an oxygen vacancy in a cubic supercell containing four formula units. The dashed band is composed of states localized at the vacancy site.

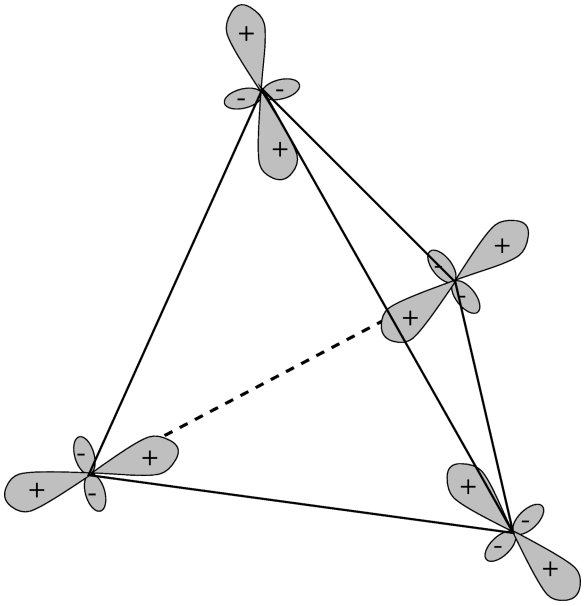

FIG. 10. Schematic representation of the Zr d orbitals that give the dominant contribution to the vacancy state.

singly degenerate vacancy state. The two electrons which once filled the O $2p$-like states in the pure crystal, and which now fill the newly created vacancy band, can be thought of as moving back to the four surrounding Zr atoms and occupying a linear combination of orbitals on the Zr atoms. Since the vacancy state at Γ belongs to the $A1$ representation of the tetragonal symmetry of the vacancy site, we can conclude that the vacancy state is a *symmetric* superposition of these four orbitals.

The vacancy state is formed as a symmetric superposition of in particular the $4d$ orbitals centered at the four Zr atoms surrounding the vacancy, as shown in Fig. 10. There are two reasons that lead to this conclusion. First, the partial density of states plot given in Fig. 11 shows that the vacancy state has very little Zr s and p character. Second, a plot of the square of the vacancy wave function (Fig. 12) shows the characteristic d_{z^2} shape around the Zr atoms. This plot also reveals that the vacancy state is indeed mostly localized on the vacancy site.

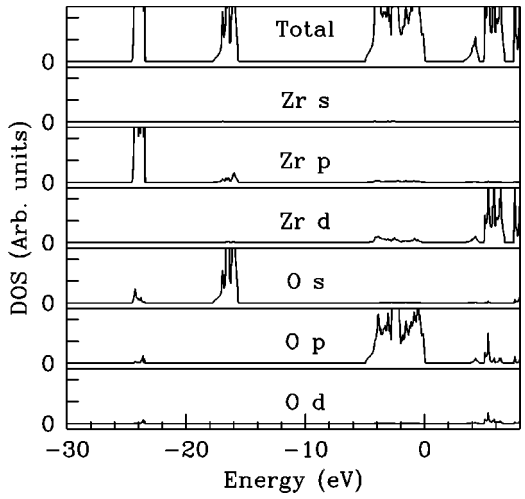

FIG. 11. Partial density of states of cubic ZrO_2 with an oxygen vacancy.

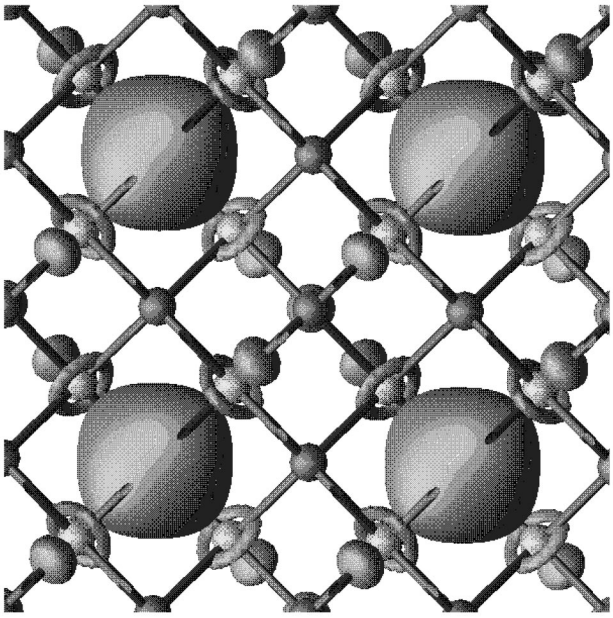

FIG. 12. Isosurface of the square of the vacancy wave function superimposed on a $2\times2\times1$ ball and stick model of the atoms and bonds. The four large balloon-shaped structures are localized on the vacancy sites and form a large part of the isosurface. The large balls adjacent to the rings and the rings themselves comprise the remaining part of the vacancy isosurface. The balls surrounded by rings are the zirconium atoms, and the tetrahedrally coordinated balls are the oxygen atoms.

In order to extract the energy of the defect level and subtract the effect of the vacancy-vacancy interaction, we model the vacancy band obtained in the supercell approach with a tight-binding model that includes the interaction of nearest and second-nearest neighbor vacancy sites. We cannot neglect the second-nearest neighbor vacancies because they are separated by only four bonds, the same number of bonds that separate the nearest neighbor vacancy sites. We neglect interactions between third-nearest neighbors in our tight-binding analysis since these are separated by six bonds.

In our supercell scheme the vacancy sites form a simple cubic lattice. Assuming first and second nearest neighbors and a single s-like ($A1$) state at the simple cubic sites, we can model the vacancy-state dispersion by

$$\begin{aligned} E(\mathbf{k}) = E_0 &+ \Delta_1[\cos(k_x a)+\cos(k_y a)+\cos(k_z a)] \\ &+ \Delta_2[\cos(k_x a)\cos(k_y a)+\cos(k_y a)\cos(k_z a) \\ &+ \cos(k_z a)\cos(k_x a)], \end{aligned} \tag{15}$$

where E_0, Δ_1, and Δ_2 are fitting parameters and a is the lattice constant of the supercell. It is possible to fit this tight-binding dispersion curve to the LDA energies of the vacancy band to better than 0.08 eV. The fact that the tight-binding dispersion curve agrees well with the LDA results shows that the vacancy-vacancy interaction is sufficiently weak and therefore that the supercell approximation is a sensible approach to the problem of determining the energy of an isolated vacancy state. The parameter E_0 is our estimate of the position of the vacancy level in the dilute limit.

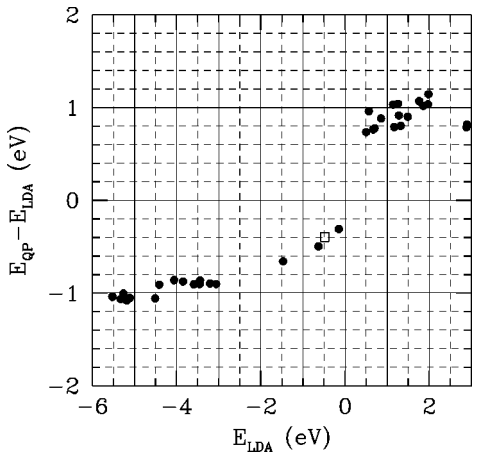

FIG. 13. *GW* quasiparticle corrections to the LDA energies for zirconia with an oxygen vacancy. The empty square shows the position of the isolated vacancy obtained from tight-binding analysis (see text).

We performed an LDA and a quasiparticle calculation of the vacancy band structure at the plane-wave cutoff of 40 Ry and a $2\times2\times2$ Monkhorst-Pack *k*-point grid. As we have seen in *GW* calculations for the pure cubic phase, this cutoff gives eigenvalues converged to better than 0.2 eV. Upon performing the tight-binding analysis outlined above, the quasiparticle vacancy level is found to be 2.1 eV below the conduction band minimum. The vacancy level, as with the bulk valence-band conduction bands, is shifted down. This is expected, since the vacancy level is occupied.

The applicability of our calculation of the oxygen vacancy state to realistic systems is limited by the fact that, in realistic doped zirconia, the oxygen vacancies are accompanied by substitutional impurities such as Ca or Y atoms on Zr sites. Indeed, if each oxygen vacancy were accompanied by one divalent (such as Ca or Mg) or two trivalent (such as Y) ions replacing Zr ions, the vacancy level would not be occupied, barring changes to the band structure. Calculations involving supercells with such impurities included are under way to assess their effect.

We also computed the quasiparticle corrections for states at high-symmetry points in the Brillouin zone for bands near the Fermi level for the vacancy supercell system. Figure 13 shows the quasiparticle correction versus the LDA eigenvalues. The bulk states exhibit quasiparticle corrections that are slightly smaller than those of the bulk cubic phase. The bulk valence to conduction band gap in this periodic array of vacancies is found to be 5.2 eV.

VI. CONCLUSION

In conclusion, we have performed full structural relaxations of the cubic, tetragonal, and monoclinic phases of zirconia within a plane-wave pseudopotential DFT-LDA method. We find excellent agreement for the structural parameters with experimental measurements and other *ab initio* calculations. We find that the relaxed crystals do have the expected total energy ordering, and the energy differences between different phases agree well with experiment.

We also performed a quasiparticle electronic-structure calculation on zirconia. The *GW* approximation employed here opens up the LDA gaps by approximately 2.3 eV throughout the Brillouin zone. We predict the fundamental gap of pure cubic, tetragonal, and monoclinic zirconia to be 5.55, 6.40, and 5.42 eV, respectively. The singly degenerate occupied oxygen vacancy level in the cubic phase is found to be 2.1 eV below the conduction band minimum.

Our studies presented here form the basis of a further investigation of the electronic properties of defects in zirconia, which are known to be responsible for the stabilization of the cubic and tetragonal phases at room temperature. In particular, supercell calculations on impurity-doped systems is envisioned. *GW* calculations on such systems could provide additional important information concerning the oxygen-ion conducting and catalytic properties of defect-stabilized cubic zirconia.

ACKNOWLEDGMENTS

The authors would like to acknowledge helpful discussions with Bernd Pfrommer and Dr. Angel Rubio. We also thank Frederic Bouyer for bringing the problem of the electronic structure of zirconia to our attention. This work was supported by National Science Foundation Grant No. DMR-9520554 and by the Director, Office of Energy Research, Office of Basic Energy Sciences, Materials Sciences Division of the U.S. Department of Energy under Contract No. DE-AC03-76SF00098. Cray C90 computer time was provided by the National Science Foundation at the Pittsburgh Supercomputer Center, the Cornell Supercomputer Center, and the NERSC Supercomputer Center.

[1] E. Ryshkewitz and D. W. Richardson, *Oxyde Ceramics. Physical Chemistry and Technology* (General Ceramics, Haskell, NJ, 1985).

[2] *Zirconia '88. Advances in Zirconia Science and Technology*, edited by S. Meriani (Elsevier, New York, 1989).

[3] R. H. French *et al.*, Phys. Rev. B **49**, 5133 (1994).

[4] R. Orlando, C. Pisani, C. Roetti, and E. V. Stefanovich, Phys. Rev. B **45**, 592 (1992).

[5] L. Hedin and S. Lundquist, in *Solid State Physics*, edited by F. Seitz, D. Turnbull, and H. Ehrenreich (Academic, New York, 1969), Vol. 23, p. 1.

[6] M. S. Hybertsen and S. G. Louie, Phys. Rev. B **34**, 5390 (1986).

[7] S. B. Zhang *et al.*, Phys. Rev. B **40**, 3162 (1989).

[8] For a recent review, see, e.g., S. G. Louie, in *Quantum Theory of Real Materials*, edited by J. R. Chelikowsky and S. G. Louie (Kluwer, Boston, 1996), p. 83.

[9] M. Rohlfing, P. Krüger, and J. Pollmann, Phys. Rev. Lett. **75**, 3489 (1995).

[10] O. Zakharov *et al.*, Phys. Rev. B **50**, 10 780 (1994).

[11] O. Zakharov, A. Rubio, and M. L. Cohen, Phys. Rev. B **51**, 4926 (1995).

[12] F. Aryasetiawan and O. Gunnarsson, Phys. Rev. Lett. **74**, 3221 (1995).

[13] P. Hohenberg and W. Kohn, Phys. Rev. **136**, B864 (1964).

[14] W. Kohn and L. J. Sham, Phys. Rev. **140**, A1133 (1965).
[15] B. Pfrommer, M. Cote, S. G. Louie, and M. L. Cohen, J. Comput. Phys. **131**, 233 (1997).
[16] N. Troullier and J. L. Martins, Phys. Rev. B **43**, 1993 (1991).
[17] D. R. Hamann, M. Schluter, and C. Chiang, Phys. Rev. Lett. **43**, 1494 (1979).
[18] L. Kleinman and D. M. Bylander, Phys. Rev. Lett. **48**, 1425 (1982).
[19] X. Gonze, P. Käckell, and M. Scheffler, Phys. Rev. B **41**, 12 264 (1990).
[20] P. Fulde, *Electron Correlations in Molecules and Solids* (Springer-Verlag, Berlin, 1991), p. 203.
[21] J. C. Phillips, Phys. Rev. **123**, 420 (1961).
[22] S. G. Louie, S. Froyen, and M. L. Cohen, Phys. Rev. B **26**, 1738 (1982).
[23] E. L. Shirley, X. Zhu, and S. G. Louie, Phys. Rev. Lett. **69**, 2955 (1992).
[24] M. Yoshimura, Am. Ceram. Soc. Bull. **67**, 1950 (1988).
[25] E. V. Stefanovich, A. L. Shluger, and C. R. Catlow, Phys. Rev. B **49**, 11 560 (1994).
[26] K. Negita, Acta Metall. **37**, 313 (1989).
[27] K. Parlinski, Z. Q. Li, and Y. Kawazoe, Phys. Rev. Lett. **78**, 4063 (1997).
[28] H. J. F. Jansen, Phys. Rev. B **43**, 7267 (1991).
[29] R. Ackermann, E. G. Rauh, and C. A. Alexander, High. Temp. Sci. **7**, 304 (1975).
[30] F. Zandiehnadem, R. A. Murray, and W. Y. Ching, Physica B & C **150**, 19 (1988).
[31] M. L. Bortz and R. H. French, Appl. Spectrosc. **43**, 1498 (1989).
[32] A. Goossens, M. Vazquez, and D. D. Macdonald, Electrochim. Acta **41**, 47 (1996).
[33] Z.-W. Lu, D. Singh, and H. Krakauer, Phys. Rev. B **36**, 7335 (1987).
[34] C. Kittel, *Introduction to Solid State Physics*, 6th ed. (Wiley, New York, 1986).
[35] B. G. Pfrommer, M. Cote, S. G. Louie, and M. L. Cohen, J. Comput. Phys. **131**, 233 (1997).